ARCHIVE OF MECHANICAL ENGINEERING

DOI: 10.24425/ame.2025.157607 2026, Vol. 73, No. 1, pp. 43–60

A.S. ABOELWAFA[1], Mahmoud Y.M. AHMED [1],
Elsayed M. KHALIL [1], Mostafa KHALIL [1]

Multi-objective trajectory optimization for guided surface-to-surface missiles

Received 26 August 2025, **Revised** 26 November 2025, **Accepted** 8 December 2025, **Published online** 20 January 2026

Keywords: trajectory optimization, tactical missile, constrained flight, control budget, optimal control, launch conditions

Guided missiles are a key weapon in modern warfare, where designers aim to enhance their accuracy and lethality. In the conceptual design phase, the problem of missile trajectory tailoring to hit a specified target emerges. Nonetheless, focusing solely on this design goal may cause degradation in other design aspects such as structural integrity and flight control demands. Therefore, it is highly recommended to integrate flight, control, and structural aspects in the early phases of design. This study focuses on the conceptual phase of a guided surface-to-surface tactical missile trajectory toward a set of predefined targets with constraints. A comprehensive analysis is implemented to solve the trajectory optimization problem of a generic tactical missile. Based on a point-mass three-degree-of-freedom flight model, the optimal-control solver GPOPS is employed to solve this trajectory optimization problem. To ensure realistic and visible trajectory problem solutions, several physical constraints are considered, including minimum and maximum allowable dynamic pressure and maximum allowable rate for flight path angle. The control budget needed for each trajectory problem is discussed. Optimal trajectories ensuring maximum impact velocity via free and constrained flights are evaluated. Furthermore, trajectory problems that balance between minimum control budget and maximum lethality are analyzed.

1. Introduction

Tactical guided missiles are a key weapon in modern warfare due to their ability to yield significant damage to ground targets with high precision. The design of such a missile is indeed multi-disciplinary since multiple possibly competing objectives are involved. It is thus recommended to incorporate more than one design objective

✉ Mostafa KHALIL, e-mail: mostafa.samir@mtc.edu.eg
[1] Aerospace Engineering Department, Military Technical College, Cairo, Egypt

in both the conceptual and preliminary design phases. Introducing as many design aspects early in these phases yields faster convergence to a more balanced final design. The development of accurate models and powerful computation facilities enabled the promotion of design optimization to the early conceptual design phase to handle competing design goals [1, 2]. The key design goals of a tactical guided missile include the impact range, velocity, and flight-path angle, which can be competing.

The trajectory optimization problem can be generally viewed as an optimal control problem. It can be expressed as a terminal cost function as the *Mayer* term [3–6], an integrand of a running cost function as the *Lagrange* term, or a *Bolza* problem with both terms (i.e., coupled *Mayer-Lagrange*) [7, 8]. Mathematically, the problem is to extremize:

$$J = \Phi_f\left(x_f, u_f, t_f\right) + \int_{t_0}^{t_f} L(x,u,t)\,\mathrm{d}t, \tag{1}$$

where, $\Phi_f\left(x_f, u_f, t_f\right)$ is the terminal cost function (*Mayer* term) of states x_f, control u_f, and time t_f, and $L(x,u,t)$ is an integrand cost function (*Lagrange* term) of states x, controls u, and time t along the trajectory.

In the early phases of solving the optimal trajectory, it is crucial to model the flying vehicle dynamics using equations of motion that incorporate assumptions customized to address the flight trajectory. Employing more complex flight models comes at a considerable time cost, yet it yields a closer approximation to realistic scenarios. Nevertheless, solving the optimal trajectory problem inherently demands substantial time due to its engagement in a rigorous iterative process, prompting the consideration of simpler flight models with suitable assumptions. Several authors have explored a two-degrees-of-freedom (2DoF) point-mass trajectory model under the assumption of a spherical, non-rotating Earth [5]. Alternatively, another study proposed the same trajectory model with a flat-Earth approximation [9]. However, the majority of authors focusing on the optimal trajectory problem have adopted a three-degrees-of-freedom (3DoF) point-mass trajectory model, assuming a spherical and rotating Earth [4, 8, 10].

Various studies from literature have been conducted to optimize flight trajectories of a variety of aerial vehicles, including commercial aircraft [11], cruise vehicles [12], unmanned aerial vehicles UAVs [13, 14], and launch vehicles. For launch vehicles, optimal flight trajectories were sought for various objectives, including maximum down-range [15], maximum cross-range [16], minimum heat-load [17], minimum fuel consumption [4, 18], maximum payload [19], and minimum flight time [20].

Trajectory tailoring is a key objective in solving trajectory optimization problems while considering constraints and in-flight limitations effectively. One widely recognized strategy in hypersonic applications is the boost-glide-skip trajectory [9, 21]. This trajectory design allows for achieving predefined range objectives, maxi-

mizing impact velocity, and mitigating excessive dynamic pressure (i.e., maintaining structural integrity) during flight.

Surface-to-surface tactical missiles have even gained the interest of many researchers, however, key gaps remain in how these studies integrate control, structural considerations, and aerodynamic constraints early in the design phase. Hargraves et al. [22] obtained the minimum time for intercepting a target for a given missile propulsion. Khalil et al. [23] solved the trajectory optimization problem maximizing the impact velocity on stationary targets. Li et al. [24] solved the Beyond Visual Range (BVR) combat missile trajectory optimization problems by maximizing range. In another study [25], the unconstrained missile trajectory optimization problem was solved to maximize the impact velocity.

As noted in [26], a hybrid trajectory optimization for variable-sweep missile configurations was developed to maximize impact velocity under constrained angle of attack and impact elevation. However, that work focused solely on the terminal phase and did not consider the integrated control–structure coupling or competing design objectives over the full flight envelope. Cai et al. [27] proposed a data-driven missile trajectory planning framework based on distributed neural networks for defense engagement scenarios. Similarly, Sun et al. [28] introduced a multi-stage trajectory optimization scheme using a hybrid multi-objective particle swarm optimization algorithm for anti-ship missiles operating in high-dynamic environments. However, both approaches not explicitly demonstrate constraint trade-offs or control–aerodynamic coupling. Additionally, a recent survey [29] on multidisciplinary design optimization (MDO) methods applied to launch vehicles during the conceptual design phase provides a broad overview of existing optimization techniques and design objectives. However, it does not address constraint formulations or trade-offs between competing objectives that are critical for practical missile trajectory design.

Given these limitations, the present study extends the existing body of work by incorporating complex interactions between optimization constraints, control objectives, and performance metrics. This integration provides a more comprehensive and realistic representation of the trajectory optimization problem. Accordingly, the trade-offs between flight range, impact velocity, summit altitude, control effort, and dynamic pressure constraints are discussed to provide a more holistic view of how these factors impact missile design during its conceptual phase. The remainder of the paper is organized as follows. Next, the case study and methodology are introduced. The results of trajectory optimization are presented and discussed. The paper finalizes the key findings and conclusions.

2. Case study

A generic missile with a tail-fin configuration is adopted as the missile under investigation, illustrated in Fig. 1a. The missile airframe has a fineness (length-to-caliber) ratio of about 15 and consists of a conical nose and a cylindrical body

ending with a four-fin tail section. The launch and burnout masses of the missile are 2800 kg and 1500 kg, respectively, and its reference area is about 0.2 m^2. Fig. 1b shows the motor thrust profile, where thrust values are normalized to their maximum value of about 280 kN. The aerodynamic drag and lift coefficients versus Mach number and angle of attack are presented in [9], where the zero-lift drag coefficient is illustrated in Fig. 2.

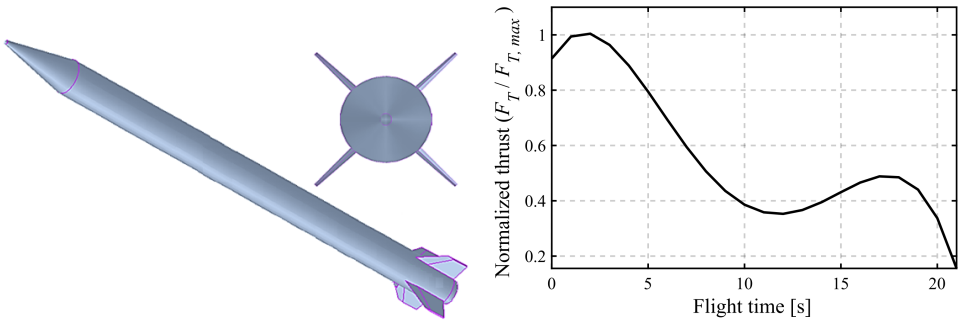

(a) configuration (b) thrust-time profile

Fig. 1. Case study missile

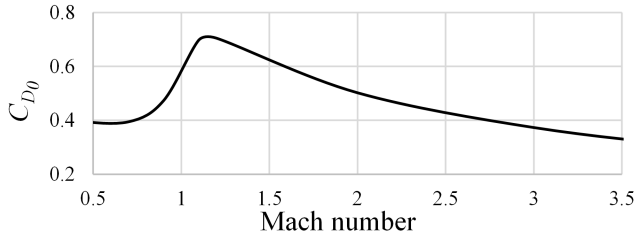

Fig. 2. Zero-lift drag coefficient vs. Mach number

The goal of the present research is to proceed with the optimal trajectories of the case study missile towards a set of predefined targets for a variety of objectives. Therefore, the trajectory model and the optimization tool implemented through this study are demonstrated below.

3. Methodology

3.1. Flight trajectory model

As illustrated in Fig. 3a, the Earth local Up-East-North coordinate system is denoted by $Mxyz$. The missile state is fully defined by the six elements $(r, \varphi, \theta, V, \Upsilon, \psi)$, namely the missile radial distance measured from Earth center, latitude, longitude, velocity, flight path angle (FPA) measured positively in the upward direction,

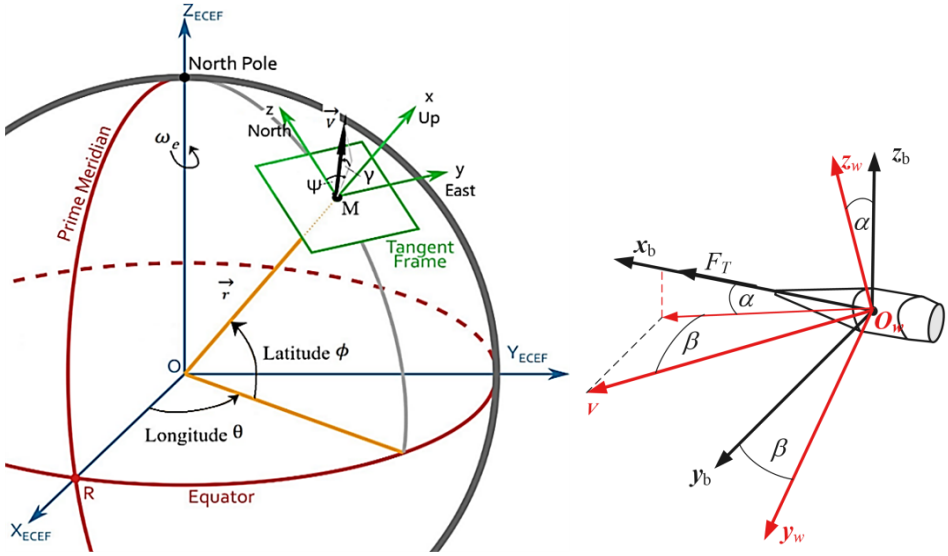

(a) (b)

Fig. 3. Coordinate systems notation

and heading angle (HA) measured positively to the right, respectively. Investigating the dynamics of guided missiles, this study assumes the neglect of the transient state resulting from control surface deflection, thereby maintaining aerodynamic moments continuously at zero, denoted as "trimmed flight". Therefore, the missile dynamics are characterized by a three-degrees-of-freedom (3DoF) point-mass motion, considering a spherical and rotating Earth. To succinctly represent these dynamics, the equations are summarized as [25],

$$\dot{r} = V \sin \Upsilon, \tag{2}$$

$$\dot{\phi} = V \cos \Upsilon \cos \psi / r, \tag{3}$$

$$\dot{\theta} = V \cos \Upsilon \sin \psi / r \cos \phi, \tag{4}$$

$$\dot{V} = \frac{F_{x_w}}{m} - g \sin \Upsilon + \omega^2 r \cos \phi \left(\sin \Upsilon \cos \phi - \cos \Upsilon \cos \psi \sin \phi \right), \tag{5}$$

$$\dot{\Upsilon} = \frac{F_{z_w}}{mV} \left(\frac{g}{V} - \frac{V}{r} \right) \cos \Upsilon + \frac{\omega^2 r}{V} \cos \phi \left(\cos \Upsilon \cos \phi + \sin \Upsilon \cos \psi \sin \phi \right) + 2\omega \cos \phi \sin \psi, \tag{6}$$

$$\dot{\psi} = \frac{-F_{y_w}}{mV \cos \Upsilon} - \frac{V}{r} \cos \Upsilon \sin \psi \tan \phi + 2\omega \left(\tan \Upsilon \cos \phi \cos \psi - \sin \phi \right) - \frac{\omega^2 r}{V \cos \Upsilon} \sin \psi \sin \phi \cos \phi, \tag{7}$$

where, m and V are the missile mass and velocity, respectively. $\omega = 7.3\times10^{-5}$ rad/s is the Earth rotation rate, $g = 9.81(R/r)^2$ is the Earth gravitational acceleration, and $R = 6378$ km is the mean Earth radius. As illustrated in Fig. 3b, F_T, L, D, and S are the missile thrust, lift, drag, and side force, respectively. α and β are the missile angle of attack (AOA) measured positively nose-up, and the sideslip angle measured positively nose-right. F_{x_w}, F_{y_w}, F_{z_w} are the missile external forces acting in the wind frame $O_w x_w y_w z_w$.

$$F_{x_w} = F_T \cos\alpha \cos\beta - D, \tag{8}$$

$$F_{y_w} = -F_T \cos\alpha \sin\beta - S, \tag{9}$$

$$F_{z_w} = F_T \sin\alpha + L. \tag{10}$$

All atmospheric properties of concern, namely, density and speed of sound, are calculated based on the US standard atmosphere 1976. The values of lift, drag, and side force coefficients are estimated using the AeroMac tool [30]. It is a semi-empirical engineering tool, developed by the research group, and validated using the same missile [31]. All calculations for aerodynamic coefficients are performed with fins in X-orientation.

3.2. Trajectory optimization tool

In this study, a commercial, well-validated non-linear MATLAB-based software GPOPS [32] is adopted to be the optimal control tool. Validation of this tool was reported by Roh et al. [33] as the optimal trajectory for a guided missile was attained. The applied trajectory optimization tool [32] employs the Radau Pseudospectral Method (RPM). Optimization tool setup includes automatic scaling. A finite-difference approach is employed for the derivatives estimation, with a mesh accuracy target of 10^{-3} and up to five refinement iterations per solution.

Computations were performed on a Dell Core i7 system with 16 GB RAM, and typical runtimes per scenario ranged from 2.5 to 8 minutes, depending on problem complexity and mesh density. Solver log files and mesh histories were reviewed to confirm convergence and solution quality.

The trajectory optimization problem includes many constraints, defining both convex and non-convex constraints [34]. Convex constraints enforce limits on dynamic pressure and load factor to ensure structure integrity, control limits in terms of the missile AOA, and other state bounds at launch, burn-out, and impact. Non-convex constraints include terminal requirements, namely the missile impact velocity and flight-path angle, and rate constraints on in-flight parameters (e.g., maximum allowable rate of change of flight-path angle and AOA). For numerical robustness, path and rate constraints were implemented directly within the transcription and monitored during mesh refinement to ensure feasibility.

3.3. Problem setup

The entire trajectory is divided into two phases, namely, active (powered) and passive (unpowered) phases. To decide the appropriate phase for flight control, numerous flight simulation trials are done with variable initial FPA (40° : 80°). Features of the resulting trajectories are compared in Fig. 4 below, showing the corresponding velocity and dynamic pressure variations with flight time. Clearly, in the active phase, the missile encounters a transonic regime (characterized by excessive drag rise) as well as extreme and abrupt variations in dynamic pressure values. To avoid these issues and the adverse impact of missile axial acceleration on control effectiveness, the control is decided to be implemented through the passive phase only. The initial FPA is limited to not exceed 70° to avoid the transonic regime flight, as inferred from Fig. 4a.

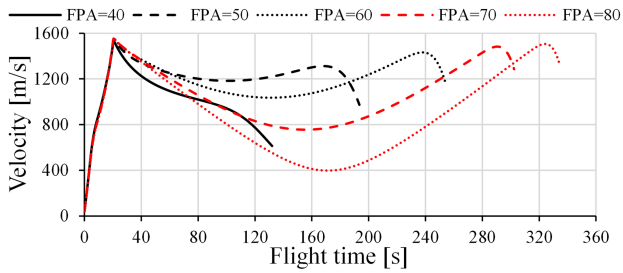

(a)

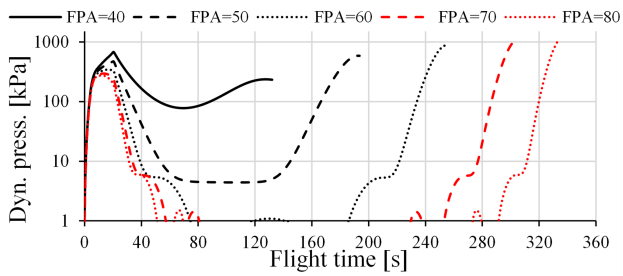

(b)

Fig. 4. Flight performance for different launch conditions (FPAs)

To ensure control effectiveness, structure integrity, and pitch-down glide maneuvers through the missile passive flight [7, 16, 35], a set of constrained flight problems is assumed. Eventually, limit values for path and control constraints in both flight phases are listed in Table 1. Eventually, three events are defined, namely, launch, burnout, and impact, defining the terminals of active and passive phases of the trajectory. The sideslip angle is set to zero over the whole flight to impose pitch-only control through this study.

Table 1. Path, and control constraint limit values

Constraint	Bounds	
	Active phase	Passive phase
AOA, α, [°]	0	$-10 \div +10$
Dynamic pressure, q [kPa]	$0.1 \div 500$	$5 \div 500$
Load factor, n [g]	$-5.0 \div +5.0$	
FPA rate of change, $\dot{\Upsilon}$ [°/s]	$-5.0 \div -0.01$	
AOA rate of change, $\dot{\alpha}$ [°/s]	0	$-5.0 \div +5.0$

3.4. Design of trajectory optimization cases

Based on the launch site (LS) data, 29.9° latitude and 32.5° longitude, eight different targets (T1–T8) were distributed arbitrarily in range and heading (measured CW from the north direction). These targets are defined as T1 (125 km, 20°), T2 (130 km, 270), T3 (150 km, 350°), T4 (165 km, 320°), T5 (175 km, 235°), T6 (185 km, 165°), T7 (220 km, 150°), and T8 (235 km, 100°). These targets are chosen such that their ranges are less than the maximum range of the missile in concern. Clearly, for unguided missiles, hitting targets located at ranges less than the maximum can be achieved by following two distinct trajectories, namely the low and high flight trajectories corresponding to the elevation of maximum range [36]. For the present study, only the low-flight trajectories are adopted for all targets of concern. In addition, only pitch control is considered. Instead of using yaw control, the launch heading angle (HA) is optimized to account for drift due to the Earth rotation.

It is important to first define the trajectories that extremize the range of the missile via both free flight OT1 and constrained flight OT2. Then, the Launch conditions are solved for both free flight OT3 and constrained OT4. Finally, the trajectory optimization problems OT5–OT7 are solved by maximizing the impact velocity and/or minimizing the control budget.

4. Results and discussion

4.1. Check of extreme ranges (OT1 and OT2)

To conclude the extreme ranges through both free and constrained flights, both optimization cases OT1 and OT2 are solved by applying the terminal cost function (*Mayer* term) listed in equation (1). As illustrated in Fig. 5, the 3D trajectory profiles for both cases indicate that the maximum and minimum ranges are consequently achieved for eastward and westward fires, respectively.

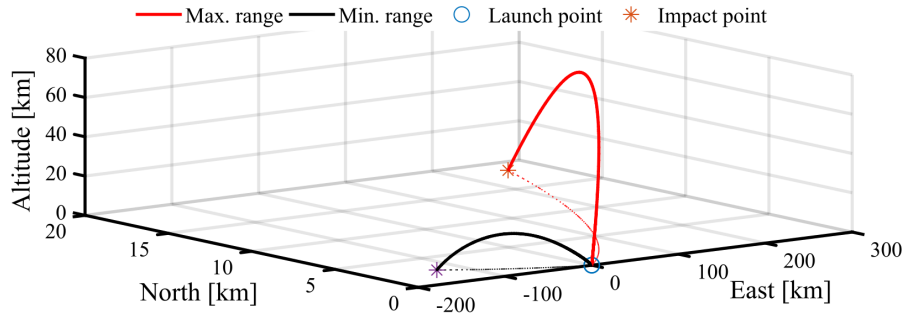

(a) OT1 case

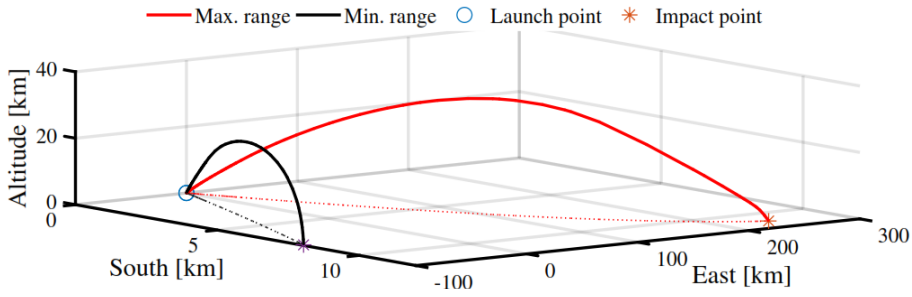

(b) OT2 case

Fig. 5. 3D trajectory profile

For the first case, OT1, the maximum range of 258.6 km is attained by launching the missile eastward with 94.95° heading (H) and an elevation of 61.12°. In contrast, the minimum range of 128.2 km is obtained by launching the missile westward with 265.13° heading and an elevation of 40°. In the second case, OT2, both extremes are obtained by launching the missile at an elevation of about 48°, satisfying the dynamic pressure bound limits as listed in Table 1.

It is noticed that, by adding control, the missile maximum and minimum ranges are decreased by 6.4% and 23.4%, respectively, which is the cost of fulfilling the safety and integrity considerations of the missile.

Fig. 6 illustrates state variations for different extreme range cases. Sharp maneuvers have been observed in the OT2 minimum range, aimed at reducing the range without violating constraints. In this scenario, most values of AOA are on the negative side (i.e., nose down, dive maneuvers), as shown in Fig. 6b. Conversely, for the OT2 maximum range, the majority of AOA values are on the positive side (i.e., glide maneuvers), directing the missile to glide through the dense atmosphere up to approximately 35 km. Finally, it is confirmed that all predefined targets of concern lie within the extreme ranges of the case study.

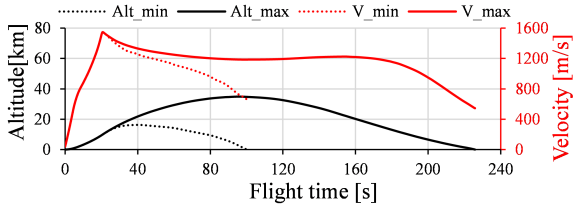

(a) Altitude and velocity

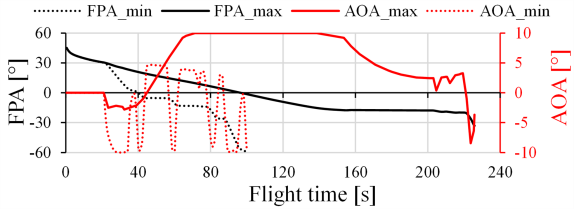

(b) Flight path angle and AOA

Fig. 6. Results for the OT2 case

4.2. Launch conditions with free flight (OT3)

The optimal trajectory problem is solved by applying the terminal cost function (*Mayer* term) for the eight predefined targets by adjusting both launch angles FPAs, and HAs. As the initial FPA is constrained to a minimum of 40°, the range of T1 is not attainable as it falls below the minimum range when accounting for Earth rotation and curvature, i.e., it is not possible to reach T1 via a free-flight. Apart from T1, the optimum initial FPA increases monotonically with the target range from 40° for T2 to about 51° for T8. In addition, as the launch FPA increases, gravity loss in vehicle velocity increases while drag loss decreases due to a sharp decrease in air density. This may explain the monotonic rise in burn-out velocity as well as summit velocity (more noticeably) and altitude with launch FPA. Finally, the deviation between impact and launch HAs increases due to the combined effects of Earth rotation and the direction of fire. More pronounced deviation concluded as both the flight time and the absolute cosine of the target azimuth increased.

4.3. Optimum launch conditions with constrained flight (OT4)

In this case, constraints are imposed as listed in Table 1, where in-flight aerodynamic control (i.e., AOA) is activated through the missile passive flight phase. The optimization problem in this case is solved to determine the launch conditions ensuring hitting the predefined targets while adhering to the imposed constraints.

Unlike in OT3 solutions, all targets (T1:T8) are reachable using a close initial FPA of about 48°, which satisfies constrained dynamic pressure as mentioned in

the OT2 problem. Hence, the corresponding summit velocities are very close with different altitudes (to satisfy the dynamic pressure constraint of 5 kPa). On the other hand, the impact velocities are also close across all targets except the minimum for the maximum range T8, indicating that the constrained dynamic pressure limits its summit. Therefore, a gliding phase is presented that degrades the missile velocity to extend the range to reach target T8. Sample optimum trajectory features for T8 are illustrated in Fig. 7. One significant remark can be addressed as the missile near the summit experiences the minimum dynamic pressure limit. To maintain an adequate lift force sufficient to glide toward the downrange T8, the AOA increases and maintains its upper bound for about sixty seconds while coasting through the summit layer.

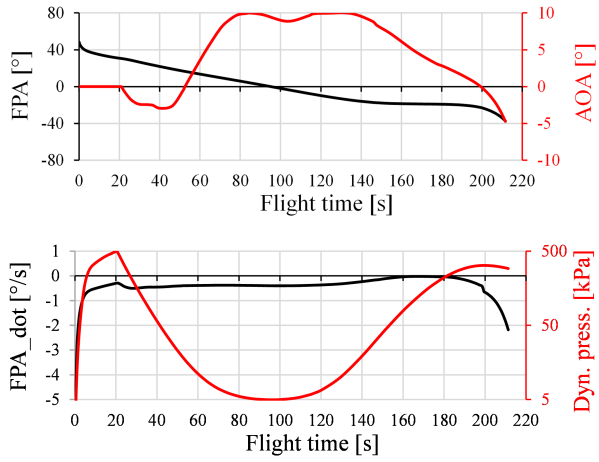

Fig. 7. Results of OT4 for the predefined target T8

4.4. Constrained flight for maximum impact velocity (OT5)

Herein, the optimized constrained trajectory problem with maximum impact velocity applying the terminal cost function (*Mayer* term) for the eight predefined targets is solved. In this problem, the launch angles that ensure hitting the target with a maximum impact velocity (i.e., maximum lethality) while satisfying the constraints are sought. It can be concluded that the maximum attainable ground impact velocity for all targets except T8 is about 900 m/s, considering the sea-level air density of 1.225 kg/m^3. The impact velocity of T8 is about 780 m/s, as the upper portion of the trajectory was constrained as a no-fly zone, restricting the flight to altitudes below approximately 35 km with a velocity of around 1200 m/s. Consequently, an extended glide phase was necessary to compensate for the resulting range shortfall, which significantly reduced the vehicle's impact speed.

The set of graphs in Fig. 8 shows the optimum constrained missile trajectory features for the target T8 as a sample. Clearly, more controller effort is needed as

compared with the OT4 case. To simultaneously obey the constraints, the additional control effort is applied in the summit layer where the dynamic pressure is minimal. This is shown by contrasting the AOA profiles for both cases in this layer.

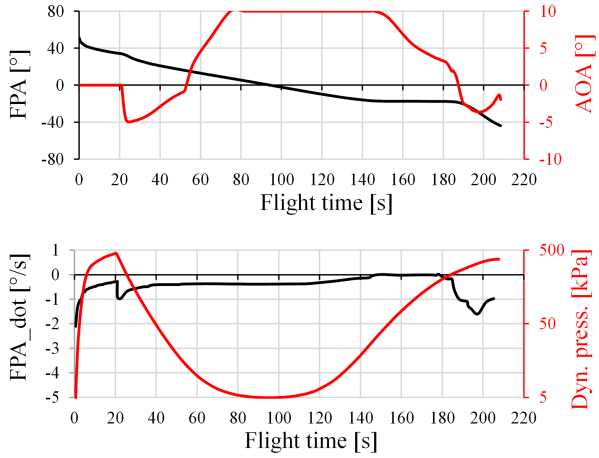

Fig. 8. Results of OT5 for the predefined target T8

4.5. Constrained flight with minimum control budget (OT6)

The focus here is drawn to flight with minimum aerodynamic control effort through missile unpowered flight. Therefore, the mean control budget through flight time is implemented as the optimizer fitness function by applying the integrand of a running cost function (*Lagrange* term), as represented by [37],

$$Q = \frac{1}{\Delta t \cdot |\alpha_{\max}|} \int_{t_b}^{t_f} \alpha(t)\,\mathrm{d}t, \tag{11}$$

where, t_b, t_f, and $\Delta t = t_f - t_b$ are the burn-out, impact, and controller application time, respectively, while $\alpha_{\max}$ is the maximum allowable AOA as listed in Table 1.

The set of graphs in Fig. 9 shows the variation of missile trajectory performance with time for the predefined target T8 as an example. As can be inferred from the above results, the need to minimize the aerodynamic control effort implies flight at a lower altitude (i.e., higher dynamic pressure) such that the control force can be attained at smaller AOA values. This can be addressed by contrasting summit conditions in OT6 with those in OT4.

As illustrated in Fig. 9, the control effort is nullified over the summit layer for about 95 seconds (from 44 to 122 seconds) while it is applied through the subsequent high dynamic pressure layers. A degradation in impact velocity emerges as a cost in OT6, as the missile coast at a lower flight altitude, causing the corresponding drag loss to increase.

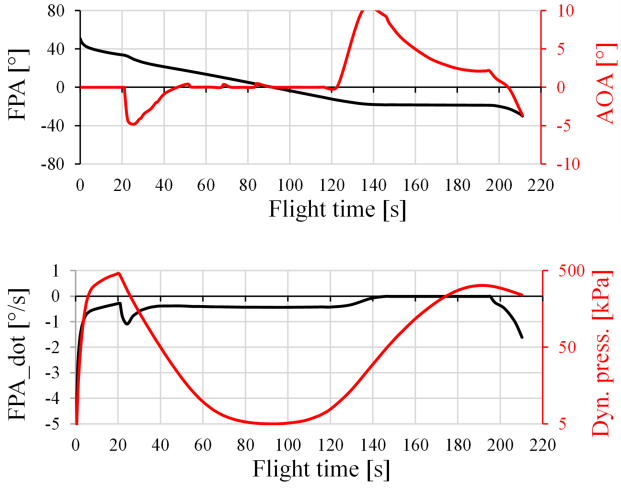

Fig. 9. Results of OT6 for the predefined target T8

4.6. Constrained flight with maximum impact velocity and minimum control effort (OT7)

Flight control aims at achieving two objectives, prioritized as follows: (1) satisfying flight constraints to achieve the required range, and (2) maximizing impact velocity with a minimum control budget (*Bolza* problem). As an example, compared to the two simulation cases, OT5 and OT6, intermediate values for the maximum impact velocity are obtained since minimizing control effort is simultaneously and equally taken into consideration. The control objective dominates over the impact velocity objective. Additionally, as concluded in Fig. 10, control commands during the coast phase have less importance than the descending phase. So, focusing control effort during the descent phase is more efficient (i.e., terminal control). This is evident in practice; for long-range guided missiles, terminal control outperforms coast control.

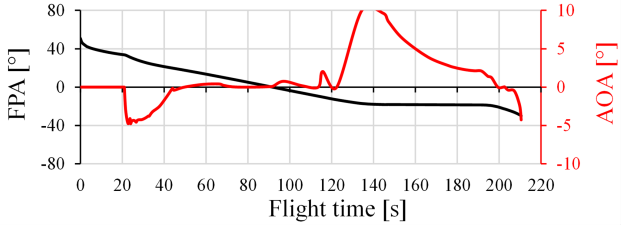

Fig. 10. Results of OT7 for the predefined target T8

4.7. Performance tradeoffs

In-flight constraints introduce performance tradeoffs while ensuring missile safety and structural integrity. Applying the free-flight solution OT3, a monotonic increase in the impact velocity with increasing the target range is experienced, as shown in Fig. 11. Nonetheless, OT4 may result in an increase or decrease in impact velocity compared to the free-flight case. This is dictated by the change in launch FPA. Therefore, maximizing impact velocity, OT5 is attained by achieving higher summit altitudes and steepening the impact FPA. Conversely, minimizing control effort, OT6 favors flight at lower altitudes, applying terminal control strategies to maximize control efficiency as in practical applications. A notable observation near the trajectory summit is that the missile encounters minimum dynamic pressure, which necessitates maintaining the angle of attack at its upper limit for extended durations to sustain lift (OT4 and OT5). This drawback is overcome in the case of minimum control effort objectives (OT6 and OT7). Furthermore, the simultaneous consideration of both objectives, OT7, negatively affects impact velocity across all ranges except the medium-range targets (T5 and T6). On the other hand, control demand increases, resulting from applying turn maneuvers to increase the FPA and hence increase gravity gain during descent flight. It is clear that the control budget, $(t_f - t_b)|\alpha_{\max}|$, was not completely exhausted for the majority of cases, as shown in Fig. 12. For instance, OT4 consumes about 40% to 60% of the control budget. For OT6 and OT7, less than 20% of the control budget is consumed.

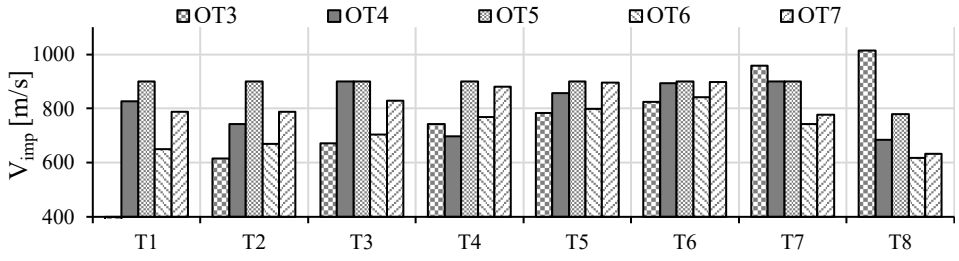

Fig. 11. Variation of impact velocity with different optimization problems

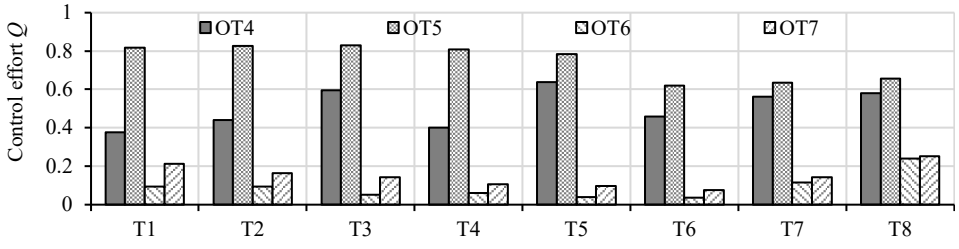

Fig. 12. Variation of the control effort with different optimization problems

It is of interest to examine the impact of reducing the AOA limits on flight performance. In addition to the original AOA limits considered above, additional simulations are conducted with reduced limits of $|\alpha_{\max}| = \pm 5^\circ$ to the cases OT4 and OT5, targeting three representative scenarios: minimum, maximum, and intermediate downrange (T4). The reduced AOA limits resulted in a new minimum and maximum downrange of 128 km and 226 km, respectively. Consequently, targets T1 and T8 become unreachable, with downrange losses of 2.4 and 3.8%, respectively, despite nearly complete utilization of the control budget (about 95% and 80%, respectively), as shown in Fig. 13.

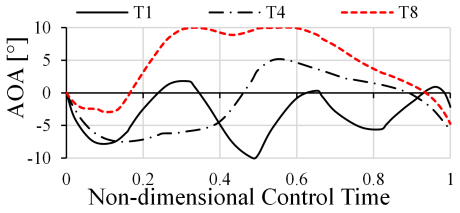

(a) AOA limits = ±10°

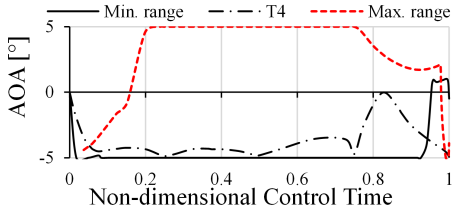

(b) AOA limits = ±5°

Fig. 13. Results of OT4 with AOA limitations

For OT5 simulations, in the case of reduced control limits, as illustrated in Fig. 14, the control budget is already fully expended to reach the constrained minimum and maximum ranges, resulting in no velocity improvement. However, for the intermediate target T4, the control effort is significantly exhausted for both OT4 and OT5 problems (about 74% and 89%, respectively), leaving less margin for in-flight disturbance mitigation.

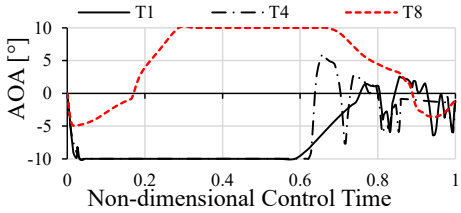

(a) AOA limits = ±10°

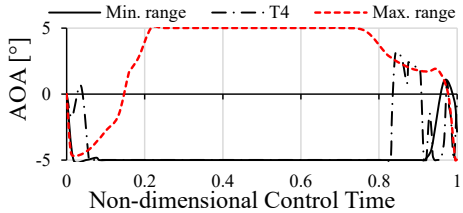

(b) AOA limits = ±5°

Fig. 14. Results of OT5 with AOA limitations

5. Conclusion

This study proposed an offline trajectory optimization framework for an aerodynamically controlled surface-to-surface tactical missile. A 3DoF point-mass motion flight model was developed and coupled with a commercial MATLAB-based

optimization tool. A total of 44 flight trajectory optimization problems are explored with different design objectives. The integration of in-flight constraints into the trajectory optimization of a tactical missile introduces notable performance tradeoffs. Adding dynamic pressure constraints leads to limiting the summit altitude of the trajectory with reduced impact velocity. The imposition of a minimum initial FPA of 40° may restrict the engagement of short-range targets, which is unattainable in a free-flight solution. The impact of Earth curvature results in nearly parabolic free-flight trajectories, while the combined effects of Earth rotation and launch azimuth increase deviations between launch and impact headings, especially when flight time and target azimuth cosine increase. Compared to free-flight trajectories, the maximum and minimum downrange for constrained flight are reduced as a mandatory cost of maintaining missile safety and structural integrity. Multiple feasible solutions are observed in constrained flight scenarios without imposing optimization objectives, reflecting the flexibility in control strategies. However, the introduction of flight control, including gliding phases and turn maneuvers, typically reduces missile velocity due to increased drag. Minimizing the control budget implies the flight at lower altitudes. This, in turn, yields lower impact velocities and hence, less lethality. The control budget is more dominant in defining the flight trajectory parameters compared to the impact velocity objective. Changing the relative weights of the two objectives may result in different impact velocity values. Building on the findings of this study, future investigations should aim to extend the presented framework to incorporate six-degree-of-freedom dynamics, aerodynamic coupling, and stochastic environmental disturbances. In addition, real-time optimization algorithms could be explored to enable adaptive trajectory updates in response to changing mission or environmental conditions.

References

[1] J.T. Betts. Survey of numerical methods for trajectory optimization. *Journal of Guidance, Control and Dynamics*, 21(2):193–207, 1998. doi: 10.2514/2.4231.

[2] A.V. Rao. A survey of numerical methods for optimal control. *Advances in the Astronautical Sciences*, 135:497–528, 2009.

[3] G.N. Kumar, M.S. Ahmed, A.K. Sarkar, and S.E. Talole. Reentry trajectory optimization using gradient free algorithms. *IFAC PapersOnLine*, 51(1):650–655, 2018. doi: 10.1016/j.ifacol.2018.05.109.

[4] R. Zardashti, M. Jafari, S.M. Hosseini, and S.A.S. Arani. Robust optimum trajectory design of a satellite launch vehicle in the presence of uncertainties. *Journal of Aerospace Technology and Management*, 12:e3520, 2020. doi: 10.5028/jatm.v12.1176.

[5] Y. Shi and Z. Wang. Onboard generation of optimal trajectories for hypersonic vehicles using deep learning. *Journal of Spacecraft and Rockets*, 58(2):400–414, 2021. doi: 10.2514/1.A34670.

[6] K. Shahzad Sana and W. Hu. Hypersonic reentry trajectory planning by using hybrid fractional-order particle swarm optimization and gravitational search algorithm. *Chinese Journal of Aeronautics*, 34(1):50–67, 2021. doi: 10.1016/j.cja.2020.09.039.

[7] E.M. Khalil, Z. Hao, and W. Chen. Missile trajectory optimization using steepest ascent method. In *Proceedings of 2013 3rd International Conference on Computer Science and Network Technology*, pages 1269–1275, Dalian, China, 12–13 October 2013. doi: 10.1109/ICCSNT.2013.6967333.

[8] J. Zhao and R. Zhou. Reentry trajectory optimization for hypersonic vehicle satisfying complex constraints. *Chinese Journal of Aeronautics*, 26(6):1544–1553, 2013. doi: 10.1016/j.cja.2013.10.009.

[9] A.S. Aboelwafa, M. Khalil, M.Y. Ahmed and E.M. Khalil. Flight path variable-fidelity modeling and optimization for supersonic autonomous guided vehicle. In *2022 4th Novel Intelligent and Leading Emerging Sciences Conference (NILES)*, pages 354–359, Giza, Egypt, 22-24 October 2022. doi: 10.1109/NILES56402.2022.9942437.

[10] Y. Cheng, S. Tang, S. Lyu, M. Wu, and H. Qiao. Aerodynamic statistics-based trajectory estimation of hypersonic maneuvering target. *IEEE Access*, 8:227642–227656, 2020. doi: 10.1109/ACCESS.2020.3044589.

[11] S. Josselyn and I.M. Ross. Rapid verification method for trajectory optimization of reentry vehicles. *Journal of Guidance, Control, and Dynamics*, 26(3):505–508, 2002. doi: 10.2514/2.5074.

[12] M. Harada and K. Bollino. Optimal trajectory of a glider in ground effect and wind shear. In *AIAA Guidance, Navigation, and Control Conference and Exhibit*, pages 1–7, San Francisco, California, 15–18 August, 2005. doi: 10.2514/6.2005-6474.

[13] R.L. Barron and C.M. Chick. Trim-reference functions for indirect method of trajectory optimization. *Journal of Guidance, Control, and Dynamics*, 30(4):1189–1193, 2007. doi: 10.2514/1.28725.

[14] X. Fang, N. Wan, H. Jafarnejadsani, D. Sun, F. Holzapfel, and N. Hovakimyan. Emergency landing trajectory optimization for a fixed wing uav under engine failure. In *AIAA Scitech Forum*, pages 1–15, San Diego, California, 7–11 January 2019. doi: 10.2514/6.2019-0959.

[15] Y. Li, N. Cui, and S. Rong. Trajectory optimization for hypersonic boost-glide missile considering aeroheating. *Aircraft Engineering and Aerospace Technology*, 81(1):3–13, 2009. doi: 10.1108/00022660910926854.

[16] Y. Li and N.G. Cui. Maximum crossrange for hypersonic boost-glide missile. In *2008 2nd International Symposium on Systems and Control in Aerospace and Astronautics*, pages 1–6, , Shenzhen, China, 10–12 December 2008. doi: 10.1109/ISSCAA.2008.4776361.

[17] Z. Wang and Y. Lu. Improved sequential convex programming algorithms for entry trajectory optimization. *Journal of Spacecraft and Rockets*, 57(6):1373–1386, 2020. doi: 10.2514/1.A34640.

[18] Y. Yang and Y. Nan. Multiphase return trajectory optimization based on hybrid algorithm. *Mathematical Problems in Engineering*, 2016:6257050, 2016. doi: 10.1155/2016/6257050.

[19] F. da Silva Mota, J.N. Hinckel, E.M. Rocco, and H. Schlingloff. Trajectory optimization of launch vehicles using object-oriented programming. *Journal of Aerospace Technology and Management*, 10:e3919, 2018. doi: 10.5028/jatm.v10.948.

[20] R.S.F. Patrón and R.M. Botez. Flight trajectory optimization through genetic algorithms for lateral and vertical integrated navigation. *Journal of Aerospace Information Systems*, 12(8):533–544, 2015. doi: 10.2514/1.I010348.

[21] P. Mesalles Ripoll, N.S. Campbell, and B. Argrow. Aerothermodynamic uncertainty in lifting and boost-glide entry trajectories. In *AIAA Scitech 2021 Forum*, pages 0934, 11–15 and 19–21 January 2021. doi: 10.2514/6.2021-0934.vid.

[22] C.R. Hargraves and S.W. Paris. Direct trajectory optimization using non-linear programming and collocation. *Journal of Guidance, Control, and Dynamics*, 10(4):338–342, 1987. doi: 10.2514/3.20223.

[23] E.M. Khalil, H. Zhou, and W. Chen. Steepest-ascent revisited: Unconstrained missile trajectory. *International Journal of Aerospace Engineering*, 2014(1):249263, 2014. doi: 10.1155/2014/249263.

[24] N. Li, H. Lei, L. Shao, T. Liu, and B. Wang. Trajectory optimization based on multi-interval mesh refinement method. *Mathematical Problems in Engineering*, 2017(1):8521368, 2017. doi: 10.1155/2017/8521368.

[25] R. Deshmukh, D.A. Spencer, and J. Longuski. Derivation of atmospheric flight equations of motion using lagrangian dynamics and its application to aerocapture. In *AIAA SciTech Forum*, pages 1-15, Orlando, FL, 6-10 January 2020. doi: 10.2514/6.2020-1742.

[26] Z. Wei, Y. Cheng, X. Guo, and S. Liu. Hybrid trajectory optimization method and tracking guidance for variable-sweep missiles. *Mathematical Problems in Engineering*, 2021:6669618, 2021. doi: 10.1155/2021/6669618.

[27] Z. Cai. Missile trajectory defense planning and data simulation based on deep learning algorithm. *Soft Computing*, 2023:1-10, 2023. doi: 10.1007/s00500-023-08907-1.

[28] J. Sun, S. You, D. Hua, Z. Xu, P. Wang, and Z. Yang. Simulation and optimization of multiphase terminal trajectory for three-dimensional anti-ship missiles based on hybrid MOPSO. *Algorithms*, 18(5):278, 2025. doi: 10.3390/a18050278.

[29] A. Oliveira and C. Cerqueira. A systematic review of mdo methods applied to launch vehicle design and their contributions to concurrent engineering. *Discover Mechanical Engineering*, 4(19):1-17, 2025. doi: 10.1007/s44245-025-00104-8.

[30] M. Khalil and M.Y. Ahmed. Flight performance and dispersion analysis for a flexible tactical missile. *Journal of Spacecraft and Rockets*, 60(4):1297–1307, 2023. doi: 10.2514/1.A35607.

[31] F. Ibrahim, M. Khalil, M.Y. Ahmed, and M. Youssef. Investigation of pitching frequency impact on stability criteria for supersonic fin stabilized missile. *Aerospace Systems*, 7(4):763–770, 2024. doi: 10.1007/s42401-024-00307-z.

[32] A.V. Rao, et.al. User's manual for GPOPS version 5.0: A MATLAB software for solving multiple-phase optimal control problems using hp-adaptive pseudospectral methods. University of Florida, Gainesville, USA, 2011.

[33] H. Roh, Y.J. Oh, M.J. Tahk, K.J. Kwon, and H.H. Kwon. L1 penalized sequential convex programming for fast trajectory optimization: With application to optimal missile guidance. *International Journal of Aeronautical and Space Sciences*, 21:493–503, 2020. doi: 10.1007/s42405-019-00230-0.

[34] Z. Wang and M.J. Grant. Constrained trajectory optimization for planetary entry via sequential convex programming. *Journal of Guidance, Control, and Dynamics*, 40(10):2603–2615, 2017. doi: 10.2514/1.G002150.

[35] G.N. Kumar, A.K. Sarkar, K.K. Mangrulkar, and S.E. Talole. Atmospheric vehicle trajectory optimization with minimum dynamic pressure constraint. *Proceedings of the Institution of Mechanical Engineers, Part G: Journal of Aerospace Engineering*, 232(5):837–846, 2017. doi: 10.1177/0954410017699436.

[36] M. Khalil. Study on modeling and production inaccuracies for artillery firing. *Archive of Mechanical Engineering*, 69(1):165–183, 2022. doi: 10.24425/ame.2021.139802.

[37] M. Bartyś and B. Hryniewicki. The trade-off between the controller effort and control quality on example of an electro-pneumatic final control element. *Actuators*, 8(1):23, 2019. doi: 10.3390/act8010023.